



Evidence of Ferromagnetism in the Diluted Magnetic Semiconductor $\text{CuGa}_{1-x}\text{Mn}_x\text{Te}_2$



José RF^{1,2*}, Carlos Durante R^{1,3} and Jaime AC¹

¹Departamento de Física, Venezuela

²Escuela de Ing Industrial, Venezuela

³Escuela de Ciencias Físicas y Matemáticas, Ecuador

*Corresponding author: José RF, Departamento de Física, Escuela de Ing Industrial, Venezuela

Submission: 📅 October 28, 2018; Published: 📅 November 30, 2018

Abstract

We report on experimental and theoretical evidence of a ferromagnetic phase in the diluted semiconductor $\text{CuGa}_{1-x}\text{Mn}_x\text{Te}_2$ using the Ferromagnetic Resonance (FMR) technique. The FMR spectra were studied as functions of temperature (T) manganese concentration (x) and magnetic field orientation. The samples were synthesized by direct fusion of the stoichiometric mixture of the elements, with Mn composition from $x=0.05$ to 0.25 . The data were interpreted in the framework of a phenomenological model for single domain uniaxial grains. The temperature variation of the resonance field shows a critical point at about 230K, which is associated with a transition from the ferromagnetic to paramagnetic state. This behaviour is explained assuming an effective magnetization following the exponential law $M(T)/M(0) = (1 - T/T_c)^\beta$, with $\beta \approx 0.40$. The resonance field as a function of the field angle displays a well-defined uniaxial symmetry at high Mn concentrations. This uniaxial field is Mn concentration dependent and is due to the formation of ovoid Mn grains with G-factor greater than 3.0.

Keywords: Magnetic semiconductors; Magnetic anisotropies; Ferromagnetic resonance; Diluted ferromagnets

Introduction

Diluted magnetic semiconductors (DMS) are alloys in which a magnetic ion is randomly distributed into the solid host and have been the subject of extensive experimental and theoretical work during the last decades [1-5]. The fundamental magnetic, electronic and optical properties of these systems are quite different from their pure semiconductor counterpart, and over the last years, it has been shown that these properties are greatly influenced by the presence of charged carriers and the localized magnetic moments of the ions, leading to strong magnetotransport and magneto-optical effects. These phenomena have been widely studied and understood in Mn-based DMS in which the magnetic moments of the Mn ions interact antiferromagnetically [6]. More recently, a new generation of transition metal-based compounds such as ZnGeP_2 [7], ZnGeSiN_2 [8], and CuAlS_2 [9], has been attracting attention because of several exciting new properties such as spin injection, carrier induced ferromagnetism, optically controlled magnetic order, etc. These materials have opened a door into the field of new magnetic materials and ferromagnetic/semiconductor hybrid structures for applications in spintronics and spin-related devices [10,11]. The main features of these alloys are the presence of vacancies, interstitial atoms, and anti-site atoms, and it is expected that when diluted into the solid matrix, the magnetic ion interacts with these defects forming pairs with low configuration energy. Theoretically, the origin of ferromagnetic ordering in DMS could be

connected to point defects responsible for the magnetic ion shelter and p-type carrier concentration induced by holes generation [12]. Experimentally, several techniques are available for studying the magnetic properties of DMS. Ferromagnetic Resonance (FMR) has proven to be one of the ideal techniques to study anisotropies and magnetic ordering in magnetic materials [13]. This is because the resonance spectrum is very sensitive to properties such as local anisotropies, magnetic interactions between intrinsic defects, and magnetic and structural inhomogeneities in the sample.

Ternary I-III-VI₂ alloys are well known by their potential applications in the photovoltaic cells, light-emitting-diodes (LEDs), and in nonlinear optical devices [14]. The most studied are those of the family Cu-III-VI, which possess high absorption coefficient [15] and energy gap near to the optimum range for conversion of solar energy [16]. Although this, the capability of diluted magnetic semiconductors of the type I-III-VI₂ as candidates for ferromagnetic/semiconductor hybrid structures is an unexplored issue. The aim of this work is addressed to test the ferromagnetic properties of the I-III-VI₂ diluted magnetic semiconductor $\text{CuGa}_{1-x}\text{Mn}_x\text{Te}_2$, by means of Ferromagnetic Resonance (FMR). The paper is organized as follows. In the section II the experimental methods are briefly described. Section III is devoted to the theoretical model used to interpret the experimental data. In section IV, our results are discussed and analyzed. In section V the main results of this work are summarized.

Experimental

Samples of the I-III-VI₂ diluted magnetic semiconductor CuGa_{1-x}Mn_xTe₂ with Mn composition x=0.05 to 0.25 were prepared by direct fusion of the stoichiometric mixture of the elements of at least 5N purity in graphite crucibles inside evacuated quartz ampoules ($\approx 10^{-6}$ Torr). To minimize the risk of explosion due to exothermic reaction between the group III element and Te, the ampoules were heated in a vertical furnace very slowly at 5K/h up to 1100 °C. Kept at this temperature for 24h, the samples were rocked at regular intervals to achieve a homogeneous mixing of the liquid phase of the reacting mixture, and then cooled to 500 °C at a rate of 5K/h. At this temperature the ampoules were annealed for 4 days. To test ferromagnetism in CuGa_{1-x}Mn_xTe₂ the ferromagnetic resonance spectrometry has been used. The ferromagnetic resonance field was measured as a function of temperature and Mn concentration, in an x-band VARIAN spectrometer, employing a homemade cylindrical cavity with Q factor of the order of 2000, adjusted in the TE₁₀₀ mode. The magnetic field is supplied by an electromagnet mounted onto a 0-360 degrees base that allowed us to rotate the sample with respect to the direction of the applied field. With this, we were able to measure the angular symmetry of the FMR signal. The magnetic field was applied parallel to the plane of the sample. All spectra were taken at 9.35GHz cavity, and in the temperature range 90 K<T<300 K. The temperature was calibrated using a carbon-glass thermometer.

Theoretical Background

The dynamics of the magnetization in a macroscopic ferromagnet is usually described using the Landau-Lifshitz-Gilbert equation (LLGE) of motion,

$$\frac{dM}{dt} = -\gamma(M \times H_{\text{eff}}) - \frac{\lambda}{M^2}(M \times M \times H_{\text{eff}}) \quad (1)$$

where M is the magnetization; $H_{\text{eff}} = -\nabla_M E$ is the effective field, E is the magnetic free energy; λ is a relaxation frequency related to the viscous damping of the magnetization; and $\gamma = 1.4g_{\text{Mn}}$ (GHz/KOe) is the gyromagnetic ratio for Mn. If our system is considered as a collection of magnetically oriented grains or particles, then the magnetic free-energy can be expressed as

$$E(\theta, \varphi) = -H_0 \cdot M + M^2 \sum_{i=1}^3 N_i m_i^2 + K \sin^2 \theta \sin^2 \varphi \quad (2)$$

where the first term is the Zeeman energy at a magnetic field H_0 , N_i are the demagnetizing factors of the material, m_i the director cosines of the magnetization M in spherical coordinates, the third term is the anisotropy energy with anisotropy constant K, and (θ, φ) are the spherical angles. At equilibrium, $(\theta = \theta_0, \varphi = \varphi_0)$, the LLGE has the periodic solution $M \exp(i\omega t)$, where ω is the resonance frequency given by the condition [17].

$$\omega^2 = \frac{\gamma^2}{M^2 \sin^2 \theta} (E_{\theta\theta} E_{\varphi\varphi} - E_{\varphi\theta}^2) \quad (3)$$

where $E_{\theta\theta}, E_{\varphi\varphi}, E_{\varphi\theta}$ are the second derivatives of the free energy evaluated at the equilibrium positions. After performing the second derivatives of the free energy, the equation (3) is written as

$$\left(\frac{\omega}{\gamma}\right)^2 = \frac{1}{\sin^2 \theta} \left\{ \left[H_0 \sin \theta_0 \cos(\varphi_0 - \varphi_H) + 2M(N_1 \cos^2 \varphi_0 + N_2 \sin^2 \varphi_0 - N_3) + E_{K\theta\theta} \right] \right. \\ \left. \times \left[H_0 \sin \theta_0 \cos(\varphi_0 - \varphi_H) + 2M(N_2 - N_1) \sin^2 \theta_0 \cos 2\varphi_0 + E_{K\varphi\varphi} \right] \right. \\ \left. - \left[H_0 \cos \theta_0 \sin(\varphi_0 - \varphi_H) + M(N_2 - N_1) \sin 2\theta_0 \sin 2\varphi_0 + E_{K\theta\varphi} \right]^2 \right\} \quad (4)$$

Here, $E_{K\theta\theta}, E_{K\varphi\varphi}, E_{K\theta\varphi}$ are the angular derivatives of the anisotropy energy evaluated at the equilibrium positions. Suppose now that our system consisted in arranged single domain uniaxial particles (grains) in the form of ellipsoids of rotation ($N_{1\perp} = N_{2\perp}$; $N_3 = N_{\parallel}$ with saturation magnetization $M = N_{\parallel} \mu_0 / V_0$, being μ_0 and V_0 the particle moment and particle volume, respectively, and anisotropy energy given by $E_K = K \sin^2 \theta \sin^2 \varphi$. The field is applied in the xy-plane parallel to the plane of the sample ($\theta_H = \pi/2$), with the magnetization along the uniaxial axis. At resonance, the magnetization follows approximately the external field so the equilibrium angles are $\theta_0 \cong \pi/2, \varphi_0 \cong \varphi_H$ so equation (4) is simplified to the form

$$\left(\frac{\omega}{\gamma}\right)^2 = \left[H_0 \cos \varphi_H - 2\epsilon M_{\text{eff}} - H_K \sin^2 \varphi_H \right] \left[H_0 \cos \varphi_H + H_K \cos 2\varphi_H \right] \quad (5)$$

which gives the resonance field for any orientation, φ_H

$$H_R = -\frac{H_1}{2} + \sqrt{\frac{H_1^2}{4} - H_2^2} \quad (6)$$

where

$$H_1 = H_K [\cos 2\varphi_H - \sin^2 \varphi_H] - 2\epsilon M_{\text{eff}}$$

$$H_2^2 = H_K^2 \cos 2\varphi_H \sin^2 \varphi_H - 2\epsilon M_{\text{eff}} H_K \cos 2\varphi_H - (\omega/\gamma)^2$$

According to this, the resonance field is uniquely determined in the range from $\varphi_0 = \varphi_H = 0$ (easy uniaxial axis) to $\varphi_0 = \varphi_H = \pi/2$ (hard uniaxial axis), such that $H_R(0) \leq H_R(\varphi_H) \leq H_R(\pi/2)$. In the case when the condition $4\pi M_{\text{eff}} \gg H_K$ is fulfilled, the FMR field is purely uniaxial and given by the simplified form

$$H_R \cong -\frac{(\omega/\gamma)^2}{2\epsilon M_{\text{eff}}} - H_K \cos 2\varphi_H \quad (8)$$

where $M_{\text{eff}} = \square N_{\parallel} - N_{\perp} \square$ is the effective magnetization, H_K is the uniaxial field defined as $2K/M$, and $\epsilon = \pm 1$ representing an ellipsoid with the shape of a spheroid (+) or an ovoid (-). Equation (8) is then compared to the experimental values of the resonance field to determine the three parameters M_{eff}, H_K and g-factor.

Results and Analysis

The FMR spectra of the sample CuGa_{0.75}Mn_{0.25}Te₂ are shown in Figure 1, for several temperatures and for a fixed field orientation. The FMR absorption is characterized by: (a) sharp low-field peak below ~ 235 K, and (b) weak high-field signal above 235K. No signal was detected for temperatures < 90 K. All signals showed asymmetrical lines-shapes which reflect some electron properties of these alloys. By rotating the plane of the sample with respect to the field direction we have studied the anisotropic properties of CuGa_xMn_{1-x}Te₂. In Figure 2 we present the angular dependence of the low-field peak recorded at $T \sim 220$ K, and for several Mn concentrations. In the sample with x=0.05 the resonance field shows no clear evidence of any anisotropy; however, a uniaxial

symmetry is observed for Mn content $x \geq 0.10$. The solid curves in Figure 3 are numerical fits of Equation (7) to the experimental data. The corresponding parameters obtained from these fits are listed in Table 1. Fairly good agreement between theory and experimental data is obtained assuming ovoid particles ($\epsilon = -1$) with g_{Mn} fixed at 3.5. This means that in average, there is an orbital contribution to the total angular momentum of Mn. It is also observed from Table 1 that both, H_k and M_{eff} , increase with Mn concentration. No angular variation was observed for the high-field peak, and it is detected in between the field range from 34400e to 36700e, depending on the Mn concentration. The temperature behaviour of the low- and high-field resonances is shown in Figure 3, for all values of x . The measurements were taken at the position of maximum resonance ($\phi_H \cong \pi/2$). The solid curve was calculated using the resonance field given in Equation (8) with $H_k(T) = H_k(0)[m(T)]^3$

and $m(T) = M_{eff}(T) / M_{eff}(0) = (1 - T/T_c)^\beta$ [18], being TC the Curie-Weiss temperature, and β a critical exponent of the order of ≈ 0.40 . For $H_k(0)$, $M(0)$ and g , we have used the values 0.10kOe, 6.6kG and 3.5, respectively. For the Curie-Weiss temperature we have used the value $T_c = 232K$, which is very close to that reported in the literature for these alloys, $T_c \approx 240K$ [19]. The dashed lines correspond to the resonance condition for a paramagnet ($H_R = \omega/\gamma$) with g -factor varying from 1.88 to 1.98, in the whole range of x . These findings are in contrast with previous works suggesting a ferromagnetic-to-superparamagnetic transition at T_c , in $CuGa_{1-x}Mn_xTe_2$ [20,21]. The behavior of the g -factor is also of interest for DMS-based spintronic devices in which relatively high effective g -factors are required and could well bear more detailed experimental attention in ferromagnetic semiconductors.

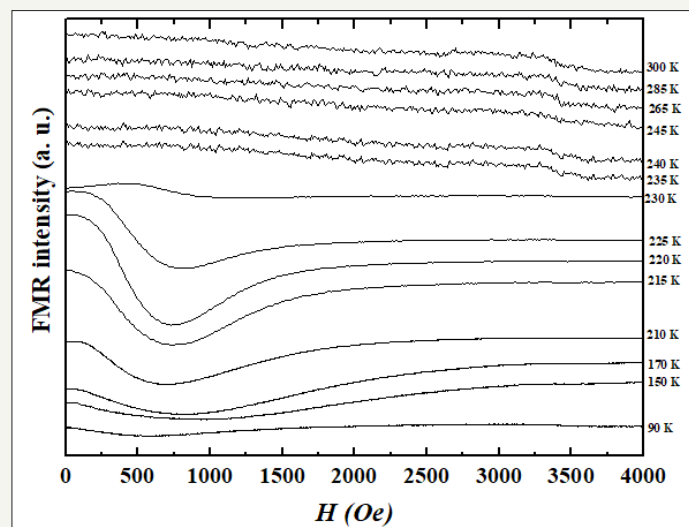


Figure 1: FMR spectra of the sample with $x=0.25$ for all temperatures. Observe the weak peak appearing at $T \approx 235$ K.

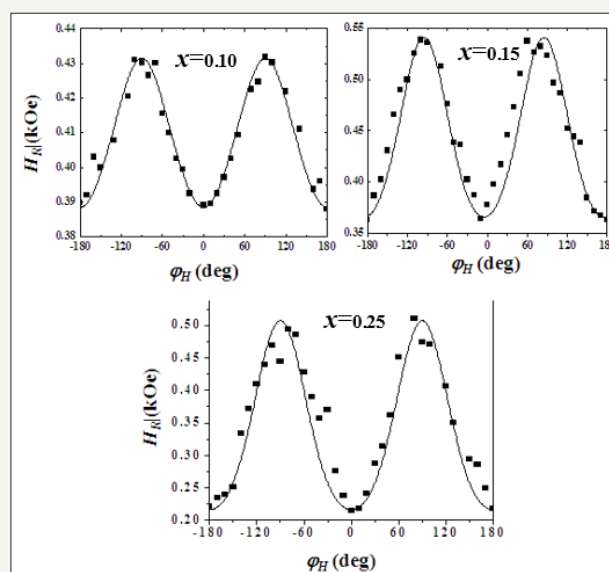


Figure 2: Angular dependence of the low-field resonance peak for: (a) $x=0.10$; (b) $x=0.15$; and (c) $x=0.25$. The measurements were performed at $T \approx 200$ K.

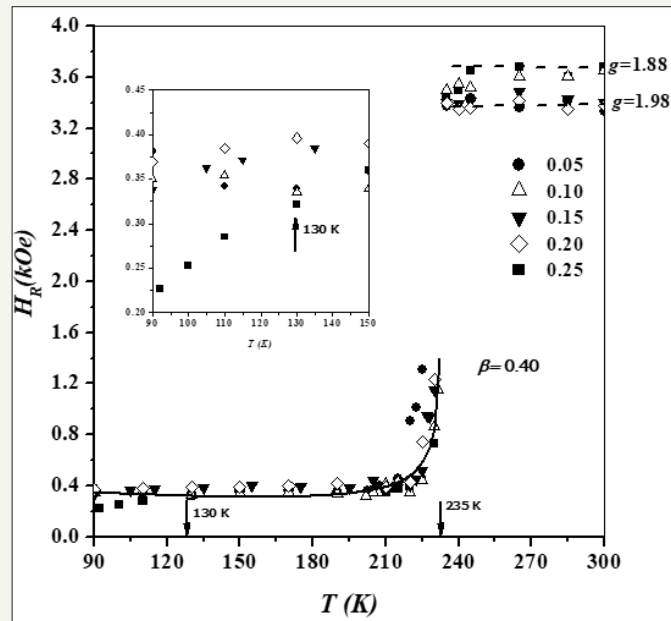


Figure 3: Temperature dependence of HR for all samples, taken with the magnetic field applied in the vicinity of maximum resonance ($\varphi H = \pi / 2$).

Table 1: Magnetic parameters of $\text{CuGa}_{1-x}\text{Mn}_x\text{Te}_2$ obtained from fitting the FMR field with Equation (7).

x	H_R (kOe)	M_{eff} (kG)	g_{Mn}
0.1	0.022	3.82	3.5
0.15	0.09	4.25	3.5
0.2	0.115	4.43	3.5
0.25	0.148	4.9	3.5

Also, of interest is the fact that in the sample with $x=0.25$ the value of HR a small shift to lower fields is observed at temperatures lower than $\sim 130\text{K}$. Qualitatively similar behavior has been reported in other Mn-based semiconductors which exhibit a ferromagnetic phase at low temperatures [22]. It has been suggested that in these materials, the ferromagnetism is mediated by holes and governed by the RKKY mechanism [23,24]. In this scenario Mn^{2+} ions substitute Ga^{3+} atoms to form the solid solution $\text{Cu}^+\text{Ga}_{1-x}^{3+}(\text{Mn}^{2+} + \bar{p})_x(\text{Te}^{2-})_2$, with a \bar{p} hole bounded to a Mn^{2+} ion at the Ga^{3+} site. At Mn concentrations $x < 0.20$, the density of holes that contribute to the effective magnetization of the Mn grains, is not sufficiently high to induce a significant increase in the magnetization, so the resonance field remains unchanged below the Curie-Weiss temperature. However, above certain Mn concentration, the density of holes increases so the magnetization of the FM grains is enhanced, and a continuous decrease in the value of HR is then observed below a critical temperature. This argument is supported by resistivity measurements which show the behavior of the density of holes with respect to temperature and Mn content in $\text{CuGa}_{1-x}\text{Mn}_x\text{Te}_2$ [20].

Conclusion

The diluted magnetic semiconductor $\text{CuGa}_{1-x}\text{Mn}_x\text{Te}_2$ was synthesized and studied the ferromagnetic properties using the FMR technique. The FM order in these materials is mainly

determined by the formation of ovoid uniaxial Mn grains with a g-factor greater than 3.0. As the temperature approaches the Curie point, the g-factor recovers the free electron value, indicative of an ordered transition from the ferromagnetic state to the paramagnetic state. This is explained assuming a particle effective magnetization satisfying the law $m(T) = (1 - T/T_c)^{\beta}$. In highly concentrated systems the FMR field shifts gradually to lower fields as the temperature is decreased below a critical value. Such a shift of the resonance field could be related to a thermal increase of the effective magnetization of the individual Mn grains. Several questions arise from this work: (a) the origin of the transition at T_c ; (b) the effect of the main grain size on the magnetic ordering; (c) the relation between the anisotropy field and the Mn concentration; (d) the real dependence of the particle magnetization with respect to temperature. Besides this, the control of the main grain size opens the possibility for manipulate the magnetic properties of Mn-doped ternary I-III-VI₂ alloys, and to increase the scientific understanding of these materials for possible use in spintronics applications.

Acknowledgement

The authors wish to acknowledge the Venezuelan institution Condes-Luz, for partially supporting this work. We also thank Dr Pedro J Silva, from the Condensed Matter Lab, IVIC, Venezuela, for technical assistance in the FMR experiments.

References

1. Furdyna J, Kossut J (1986) Diluted magnetic semiconductors, semiconductors and semimetals. Academic Press, Vol. 25, Boston, USA.
2. Freeman J, Zhao YJ (2003) Advanced tetrahedrally-bonded magnetic semiconductors for spintronic applications. J Phys Chem Solids 64(9-10): 1453-1459.
3. Diwekar M, Borchers JA, Donovan KVO, Halperin J, Awschalom DD, et al. (2004) Magnetic properties of (Ga,Mn) as digital ferromagnetic heterostructures. J Appl Phys 95(11): 6509

4. Gavriljuk VG, Dobrinsky A, Shanina BD, Kolesnik SP (2006) A study of the magnetic resonance in a single-crystal Ni(50.47) Mn(28.17) Ga(21.36) alloy. *J Phys Condens Matter* 18(32): 7613-7627.
5. Zutic, Fabian J, Das Sarma S (2006) Spintronics: Fundamentals and applications. *Rev Mod Phys* 76: 165-203.
6. McCarty D, Hassan AK, Brunel LC, Dziatkowski K, Furdyna JK (2005) Electron paramagnetic resonance shift in $\text{II}_{1-x}\text{Mn}_x\text{VI}$ diluted magnetic semiconductors in the presence of strong exchange coupling. *Phys Rev Lett* 95: 157201-1.
7. Cho S (2002) *Phys Rev B* 65: 257203.
8. Pearton SJ, Abernathy CR, Overberg ME, Thaler GT, Norton DP (2003) Wide band gap ferromagnetic semiconductors and oxides *Journal of Applied Physics* 93(1): 10.1063-1.1517164.
9. Chu, Osinsky A, Fuflyigin V, Zhu LD, Polyakov AY, et al. (2002) Magnetic and structural characterization of Mn-implanted, single-crystal ZnGeSiN_2 . *J Appl Phys* 92: 2047.
10. Freeman YJ, Magn J (2002) First-principles prediction of a new class of ferromagnetic semiconductors. *Magn Mater* 246(1-2): 145.
11. Ohno H (1998) Making nonmagnetic semiconductors ferromagnetic. *Science* 281(5379): 951-955.
12. Redinski P, Rappoport TG, Libal A, Furdyna JK, Jankó B, et al. (2005) Optical response of a ferromagnetic-diluted magnetic semiconductor hybrid structure. *Appl Phys Lett* 86: 113103.
13. Zhao YJ, Alex Z (2004) Electronic structure and ferromagnetism of Mn-substituted CuAlS_2 , CuGaS_2 , CuInS_2 , CuGaSe_2 and CuGaTe_2 *Phys Rev B* 69(10): 104422
14. Michael Farle (1998) Ferromagnetic resonance of ultrathin metallic layers. *Rep Prog Phys* 61(7): 755.
15. Rockett RW, Birkmire J (1991) CuInSe_2 for photovoltaic applications. *Appl Phys* 70(7): 10.1063-1.349175.
16. Hovel HJ (1975) Semiconductors and semimetals. In: Willardson K, Beer AC (Eds.), *Solar Cells*, Acad Press, NY, USA, 2: 71-92.
17. Chopra L, Tiwari AN (1987) Ternary and multinary compounds. In: Deb SK, Zunger A (Eds.), *Materials Research Society*, USA, p. 49.
18. Suhl H (1955) Ferromagnetic resonance in nickel ferrite between one and two kilomegacycles. *Phys Rev* 95(2): 555.
19. Callen HB, Callen E (1966) The present status of the temperature dependence of magnetocrystalline anisotropy, and the $1(1+1)2$ power law. *J Phys Chem Solids* 27(8): 1271-1285.
20. Lee WL, Pray T, Regan KA, Cava RJ, Bhatt RN, et al. (2002) APS March Meeting U16.4, Indianapolis, USA.
21. Novotortsev VM, Shabunina GG, Koroleva LI, Aminov TG, Demin RV, et al. (2007) Superparamagnetism in Mn-doped CuGaTe_2 . *Inorganic Materials* 43(1): 12-17.
22. Pérez, Silva PJ, Rincón CA, Ferrer JP, Fermin JR (2008) EPR study of the diluted magnetic semiconductor $\text{CuGa}_{1-x}\text{Mn}_x\text{Te}_2$. *J Magn Magn Mater* 320(17): 2155-2158.
23. Story T, Eggenkamp PJT, Swuste CHW, Swagten HJM, Szczerbakow A, et al. (1993) Magnetic-resonance study of the diluted magnetic semiconductor $\text{Pb}_{1-x-y}\text{Sn}_y\text{Mn}_x\text{Te}$. *Phys Rev B* 47(1): 227.
24. Dietl T, Ohno H, Matsukura F, Cibert J, Ferrand D (2000) Zener model description of ferromagnetism in zinc-blende magnetic semiconductors. *Science* 287(5455): 1019-1022.



Creative Commons Attribution 4.0 International License

For possible submissions Click Here

Submit Article



Research & Development in Material Science

Benefits of Publishing with us

- High-level peer review and editorial services
- Freely accessible online immediately upon publication
- Authors retain the copyright to their work
- Licensing it under a Creative Commons license
- Visibility through different online platforms